JOURNAL OF AGRICULTURAL AND FOOD CHEMISTRY
ARTICLE

J. Agric. Food Chem. 2011, 59, 577–583 577
DOI:10.1021/jf103957k

Proteomic Analysis of Up-accumulated Proteins Associated with Fruit Quality during Autumn Olive (*Elaeagnus umbellata*) Fruit Ripening

Man-Cheng Wu, Hai-Tao Hu, Li Yang, and Ling Yang*

College of Chemistry and Life Sciences, Zhejiang Normal University, Jinhua, Zhejiang 321004, China

Fruit ripening is a complex phenomenon that makes berries attractive and also determines their nutritional value. Autumn olive (*Elaeagnus umbellata* Thunb.) fruit is a rich source of many human health-related nutrients. The changes in pericarp color are initiated at early developmental stages, coinciding with the fast increase in fruit size. Fruit quality traits with special emphasis on soluble sugars, organic acids, lycopene, and total protein contents were assayed during the fruit ripening. In the fully ripe fruit, glucose and fructose were the principal sugars, malic acid was the most abundant organic acid, and lycopene concentration was extremely high. A proteomic analysis was used to identify up-accumulated proteins induced by the ripening. Among 63 up-accumulated protein spots, 43 were successfully identified by MALDI-TOF/TOF-MS. All 43 proteins were novel for autumn olive, and 8 were first reported in the fruit. Twenty-one proteins of known function were involved in sugar metabolism, citric acid cycle, isoprenoid metabolism, fatty acid synthesis, and protein hydrolysis. The possible roles of these 21 accumulated proteins in autumn olive fruit quality are discussed.

KEYWORDS: Autumn olive; fruit quality; ripening; proteomics; up-accumulated protein

INTRODUCTION

Autumn olive (*Elaeagnus umbellata* Thunb.) is a vigorous shrub. Due to its ability to fix nitrogen, drought and disease resistance, and tolerance of poor soil, autumn olive has been widely planted to prevent erosion and provide screening along highways (*1*). Its red fruit is rich in minerals, vitamins, essential fatty acids, flavonoids, and carotenoids (*2*), especially lycopene, which is about 5−20 times higher than that of ordinary tomato (*1*,*3*). The sweet-tart fruit can be eaten fresh or processed for preserves, condiments, and fruit rolls and juice or used as a substitute for tomato products (*1*, *2*). Although the fruit is eaten in Asia, autumn olive is not yet popular and widely cultivated for its edible fruit (*1*). This nutritional fruit may have a broad prospect in healthcare food and clinical application (*1*−*3*).

Fruit ripening is highly coordinated, genetically programmed, and an irreversible phenomenon involving a complex series of physiological and biochemical events (*4*). The metabolic changes vary among species and generally include pigment biosynthesis, conversion of starch to sugar, and accumulation of flavor and aromatic volatiles, eventually making the fruit attractive, tasty, and nutritious (*5*). The main characteristics related to fruit quality are color, taste, texture, and nutrition, which can be assessed indirectly by measuring some parameters such as soluble sugars, organic acids, and antioxidant contents (*6*, *7*). In contrast to well-studied fruits such as tomato (*5*), apple (*8*), grape (*9*, *10*), and citrus (*11*), little is known about the changes in the content of compounds related to fruit quality as autumn olive ripening processes advance. Very limited genomic information is available on this species; only 53 nucleotide, 177 EST, and 55 protein sequences are reported in the NCBI database (June 10, 2010). A deeper understanding of the mechanisms underlying fruit ripening is highly desirable for possible manipulations aimed at improving the edible quality.

Proteomics offers a powerful approach to examine simultaneous changes and to classify temporal patterns of protein accumulation occurring in complex ripening processes (*8*−*12*). Functional proteomics can be used to screen and identify proteins involved in specific metabolic networks. Compared with the mRNA level, the protein level integrates post-transcriptional and post-translational processing that regulates the localization, quantity, and efficiency of the final product in the cell (*12*). In recent years, the proteomic technique has been successfully applied to the protein expression changes during fruit ripening in many fruit species including citrus (*11*), apple flesh (*8*), cherry tomato pericarp (*12*), and grape berry tissues (*9*). The results in part confirmed transcriptomic data, but in many cases diverged from gene expression data or uncovered the evolution of proteins for which gene expression was not profiled. In this study, we report the first proteomic analysis of autumn olive pulp. Our main objectives were to (i) identify significantly up-accumulated proteins during the fruit ripening and (ii) link the protein variations with some chemical constituents related to fruit quality.

MATERIALS AND METHODS

Plant Materials. Autumn olive (*E. umbellata* Thunb.) fruits were harvested during the 2008 growing season from the experimental orchard of Zhejiang Normal University. The diameter of three fruit was measured

*Corresponding author (phone +86-579-82282396; fax +86-579-82280322; e-mail yangl@zjnu.cn).

Published on Web 12/22/2010

once every other week to assess fruit growth in a nondestructive manner. The evaluation of fruit maturity was based on pericarp color and fruit development time post fertilization. Three hundred fruits from three plants were collected in accordance with homogeneous size and color at each sampling date and then were immediately pitted and frozen in liquid nitrogen for biochemical and proteomic analysis.

Determination of Sugar and Organic Acid Concentration. The frozen sample of 20 fruit pulps was pulverized in liquid nitrogen and then subjected to sugar and organic acid extraction. HPLC was carried out on a Waters system (Waters 600) as previously described (*13*). Sugars were analyzed using a Polyspher CH PB column (300 × 7.8 mm) (Merck, Darmstadt, Germany) and a Waters 2410 refractive index detector. The mobile phase was deionized water, and the flow rate was 0.4 mL/min. Organic acids were determined using a Lichrospher 100 ODS column (125 × 4 mm) (Merck) with 0.05 M KH_2PO_4 (pH 2.6) as the mobile phase at a flow rate of 0.6 mL/min. The Waters 2487 UV−vis detector was set at 214 nm. The individual sugars and organic acids were identified by comparing retention times with those of authentic standards. All reference standards were purchased from Sigma (St. Louis, MO). The total sugar or organic acid content was the sum of identified sugars or organic acids. At least three replications (3 × 20 fruits) were performed for each ripening stage. Data were expressed as mean ± SE ($n = 3$) and statistically analyzed by SPSS version 12.0 software for Windows. One-way ANOVA followed by *t* test was applied to determine the significant difference between green and fully ripe groups at the level of $p < 0.05$.

Protein Extraction. About 1 g of fine powder from 20 fruit pulps was suspended in 2.5 mL of cold extraction buffer (0.9 M sucrose, 0.1 M Tris-HCl, pH 8.8, 10 mM EDTA, 200 mM KCl, and 2% w/v DTT), vortexed, and incubated for 30 min on ice. After the addition of an equal volume of phenol saturated with 0.1 M Tris-HCl, pH 8.8, the mixture was shaken for 30 min and then centrifuged at 20000*g* for 15 min at 4 °C. The phenol phase was reextracted twice with the extraction buffer. Proteins were precipitated by the addition of 5 volumes of saturated ammonium acetate in methanol, left overnight at −20 °C, and centrifuged at 20000*g* for 15 min. The protein pellets were then washed with cold saturated ammonium acetate in methanol, 70% ethanol, and acetone, respectively. The final pellet was air-dried for 30 min at 4 °C and dissolved in lysis buffer (8 M urea, 2 M thiourea, 2% w/v CHAPS, 50 mM DTT, 2% v/v Triton X-100, and 0.5% w/v ampholytes, pH 3−10). The protein concentration was determined by using the Bradford assay with BSA as standard. Three separate extractions were done for each ripening stage.

2-DE and Image Analysis. 2-DE separation of green and fully ripe fruit proteins was performed as previously described (*14*), and 200 μg of proteins was loaded per gel. At least four gels for each extraction were silver stained using a modified protocol (*15*) and scanned at 400 dots per inch resolution with a UMAX Power Look 2100XL scanner (Maxium Tech., Taipei, China). The images were analyzed with PDQuest 7.3 software (Bio-Rad). Spot detection and matching between gels were performed automatically followed by manual verification. After normalization of the spot densities against the whole-gel densities, the percentage volume of each spot was averaged for at least nine different gels of three separate extractions. Student's *t* test analysis of green versus fully ripe fruit gels was performed for each independent replicate experiment. Only reproducible changes statistically detected for the three experiments were considered to be differentially accumulated proteins.

In-Gel Digestion and Mass Spectrometric Analysis. Protein spots were washed twice with pure water and destained in a 1:1 solution of 30 mM potassium ferricyanide and 100 mM ammonium bicarbonate. The gel pieces were subsequently dehydrated and rehydated with ACN and sequencing grade porcine trypsin (Promega, Madison, WI) solution (20 μg/mL in 25 mM NH_4HCO_3). Following 16 h of digestion at 37 °C, tryptic peptides were extracted twice with 67% ACN containing 1% trifluoroacetic acid and then completely dehydrated in a vacuum centrifuge and resuspended in 5 μL of 0.1% trifluoroacetic acid. Samples were mixed 1:1 with matrix solution containing 50% ACN and 0.1% trifluoroacetic acid saturated with α-cyano-4-hydroxycinnamic acid and spotted onto sample plates.

The peptide mixtures were analyzed on a 4800 MALDI-TOF/TOF mass spectrometer (Applied Biosystem Sciex, Foster City, CA). Before each analysis, the instrument was calibrated using a CalMix5 standard (ABI4700 Calibration Mixture). Acquisitions were performed in positive ion reflectron mode. The MS spectrum was generated by averaging 800 laser shots over the mass range m/z 800−3500 Da, and the eight most intense precursor ions were selected for subsequent MS/MS fragmentation. Ion activation was achieved using 1 kV collision-induced dissociation with air as the collision gas. Sixteen hundred laser shots were averaged for each MS/MS spectrum. The peaks were deisotoped, and only those with s/n ≥ 10 in a MS spectrum and with s/n ≥ 5 in a MS/MS spectrum were retained for interpretation.

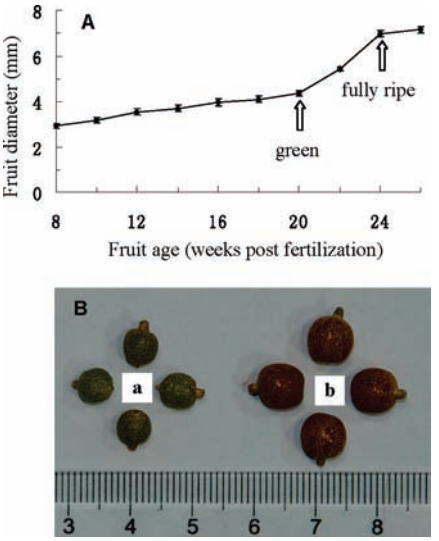

Figure 1. (**A**) Autumn olive fruit growth estimated by measurement of equatorial fruit diameter ($n = 3$); (**B**) green fruit (a) and fully ripe fruit (b) used for proteomic analysis.

Database Search. Data were preprocessed by the manufacturer computer program GPS Explorer version 3.6 (Applied Biosystems), and automated database searching was carried out using the MASCOT search engine version 2.1 (Matrix Science, London, U.K.). Combined MS−MS/MS searches were conducted with selection of the following criteria: NCBInr database (release 20080910; 7241274 sequences; 2502556391 residues), taxonomy of Viridiplantae (green plants), trypsin digestion, one missed cleavage, partial modification of cysteine carboamidomethylation and methionine oxidation, no fixed modifications, parent ion mass tolerance at 60 ppm, and MS/MS mass tolerance of 0.25 Da. The probability score (95% confidence level) calculated by the software was initially used as criteria for correct identification.

RESULTS AND DISCUSSION

Determination of the Developmental Stages of Autumn Olive Fruit. We followed fruit growth by measuring the equatorial fruit diameter (**Figure 1A**). Intensive fruit growth started at 20 weeks post fertilization and reached a plateau at 24 weeks post fertilization. Mean fruit size increased from 4.37 ± 0.12 mm at green stage to 6.99 ± 0.13 mm at fully ripe stage. Pericarp color changes are initiated at early developmental phases and coincided with this rapid growth period (**Figure 1B**), which were similar to those found in nonclimacteric cherry fruit (*7*). Furthermore, profound changes in chemical compositions occurred. The sugar content increased from 10.03 to 97.00 mg/g fresh weight (**Table 1**). All of these are characteristics of fruit ripening (*10*). Sampling for this proteomic study was performed at green stage (20 weeks post fertilization) and fully ripe stage (24 weeks post fertilization with full red color) (**Figure 1B**) to identify proteins linked to chemical compositions during autumn olive fruit ripening.

Proteomic Responses during Autumn Olive Fruit Ripening. Extraction of proteins suitable for 2-DE from autumn olive fruit proved to be challenging. Autumn olive pulp is a recalcitrant tissue for proteomic analysis, due to a low protein content and high concentration of interfering compositions such as organic

Table 1. Sugar and Organic Acid Content (Fresh Weight Basis) at Two Autumn Olive Fruit Ripening Stages

	sugars[a] (mg/g) (mean ± SE)				organic acids[a] (mg/g) (mean ± SE)				
ripening stage	glucose	fructose	sucrose	total sugars	malic acid	citric acid	lactic acid	tartaric acid	total acids
green	4.62 ± 0.39	5.34 ± 0.05	0.07 ± 0.001	10.03 ± 0.46	12.81 ± 0.38	5.88 ± 0.19	2.76 ± 0.29	3.76 ± 0.22	25.21 ± 0.92
fully ripe	48.42 ± 0.57**	47.03 ± 0.19**	1.55 ± 0.37**	97.00 ± 0.79	13.60 ± 1.42	7.88 ± 0.57**	3.28 ± 0.49	1.83 ± 0.46*	26.59 ± 1.63

[a] * and ** indicate significance level at $p < 0.05$ and $p < 0.01$, respectively.

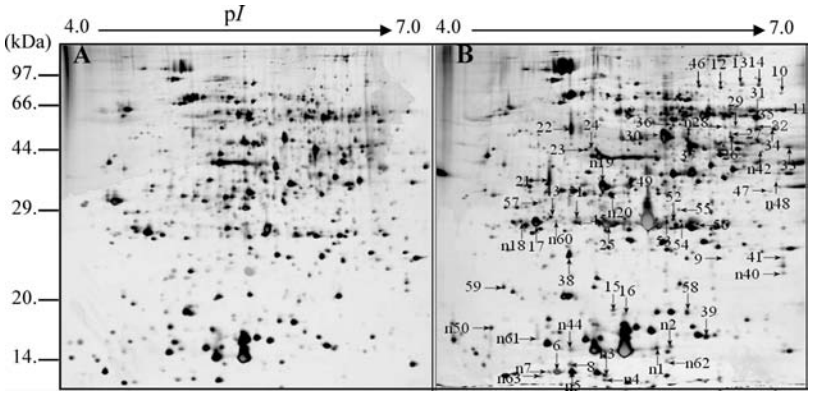

Figure 2. Representative 2-DE gels of autumn olive fruit proteins at two ripening stages: (**A**) green fruit; (**B**) fully ripe fruit. Forty-three successfully identified and 20 no-matched (labeled "n") spots, all of which were up-accumulated during the ripening, are indicated on the map of fully ripe fruit sample (**B**).

acids, carbohydrates, phenols, and terpenoids (*1*−*3*). Phenol extraction followed by ammonium acetate/methanol precipitation gave the best quality and yield. The representative 2-DE maps are shown in **Figure 2**. The average number of detected spots was about 1030 and did not vary significantly between the two stages. Quantitative image analysis revealed that 79 protein spots (about 8%) were differentially accumulated by >2-fold ($p < 0.01$) in the fully ripe fruit compared with the green fruit. This percentage was similar to that of ripening tomato pericarp (*12*). Sixty-three protein spots were up-accumulated during autumn olive fruit ripening, and 6 of them (spots 36, 47, 58, 10, 9, and 49) were detected only in the fully ripe fruit (**Table 2**). The amount of up-accumulated protein spots was nearly 4-fold that of down-accumulated spots. In this study, we focused on up-accumulated protein spots, expecting to identify the candidate proteins involved in active nutrition accumulation induced by fruit ripening.

Identification of Up-accumulated Protein Spots. Among 63 up-accumulated protein spots, 43 were identified by MALDI-TOF/TOF MS (**Table 2**; see also the Supporting Information), and the identification success rate was 68%. The remaining protein spots presented no homology with sequences available in the databases (labeled "n" in **Figure 2**), which can largely be attributed to the low abundances of these spots. Among the 43 identified spots, 10 corresponded to *Arabidopsis thaliana* sequences, 10 to *Oryza sativa* sequences, 3 each to *Pisum sativum* and *Populus* sequences, and the remaining 17 to more phylogenetically distant species. All of them were novel proteins for autumn olive, and eight (dimethylmenaquinone methyltransferase, metallopeptidase, 26S proteasome regulatory subunit rpn11, secoisolariciresinol dehydrogenase, hypersensitive induced reaction 3, chaperonin TCP-1, 2-isopropylmalate synthase A, and an unknown protein) were first reported in the fruit.

The functional classification of the identified proteins was performed according to MIPS FunCat annotation and is shown in **Table 2**. Most of the up-accumulated proteins were related to defense response (23.2%), whereas five (11.6%) were known to be involved in the oxidative stress response. Defense response and oxidative process were common physiological events during fruit ripening (*5*, *8*−*10*). The percentage of proteins involved in sugar metabolism (16.3%) was also noteworthy. The 21 proteins listed as the first five functional categories in **Table 2** were related to fruit quality.

Proteins Involved with Sugar Metabolism. Soluble sugar content is a primary criterion in evaluating fruit quality (*2*). Glucose, fructose, and sucrose were detected in green autumn olive fruit, and all three sugar contents increased significantly ($p < 0.01$) with ripening. Glucose and fructose were the predominant soluble sugars in the fully ripe autumn olive fruit (**Table 1**), which were also observed in the sweet cherry (*7*). Total soluble sugar was 97.00 mg/g fresh weight of fruits, which was much higher than tomato (*16*, *17*), but lower than sweet cherry (*7*). The presence of large amounts of sugar in autumn olive fruit not only is important for its direct use as a fruit or in the form of juice and other byproducts but also can increase the shelf life, suggesting a better potential for market value (*2*).

Seven protein spots, namely, α-amylase (spot 30), UGPase (spots 31 and 35), phosphoglucomutase (spot 12), acid invertase (spots 21 and 22), and triose-phosphate isomerase (spot 56), were involved in sugar metabolism (**Table 2**). The vacuolar located acid invertase (EC 3.2.1.26) catalyzes the hydrolysis of sucrose into glucose and fructose in equal proportions (*18*). When an acid invertase gene was antisense suppressed in muskmelon, the sucrose concentration increased in transgenic fruit (*19*). Two isoforms of acid invertase identified in this case were strongly up-accumulated >7-fold during the ripening (**Table 2**). This suggests acid invertase could be a key enzyme that made both glucose and fructose become the main sugars in the fully ripe autumn olive fruit (**Table 1**).

α-Amylase (EC 3.2.1.1) has endoglycolytic activity on the α-1,4-D-glucosidic linkages randomly within starch and oligosaccharide chains, ultimately yielding the reducing sugar (*20*). UGPase (EC 2.7.7.9) is an enzyme catalyzing the reversible conversion between glucose 1-phosphate and UDPglucose (*11*). Phosphoglucomutase (EC 5.4.2.2) interconverts the 1- and

Table 2. Up-accumulated Proteins during Autumn Olive Fruit Ripening

spot	protein name	GenBank gi	organism	theor M_r/p*I*	exptl M_r/p*I*	relative change [a]
			Sugar Metabolism (16.3%) [b]			
12	cytosolic phosphoglucomutase	40233152	*Populus tomentosa*	63.22/5.49	13.22/6.39	3.46 ± 0.51
21	vacuolar acid invertase Psl-1	21464543	*Pisum sativum*	71.96/6.11	33.59/5.05	8.36 ± 0.47
22	acid invertase	21745136	*Lagenaria siceraria*	74.00/5.46	45.61/5.32	7.46 ± 0.11
30	α-amylase precursor	22536012	*Musa acuminate*	46.77/5.83	43.26/5.95	2.20 ± 0.24
31	UDP-glucose pyrophosphorylase, UGPase	17026394	*Amorpha fruticosa*	51.55/6.07	51.91/6.66	3.12 ± 0.04
35	UDP-glucose pyrophosphorylase, UGPase	17026394	*Amorpha fruticosa*	51.55/6.07	51.93/6.45	6.34 ± 1.44
56	triosephosphate isomerase	57283985	*Phaseolus vulgaris*	27.18/5.87	26.74/5.22	2.65 ± 0.42
			Citric Acid Cycle (9.3%)			
11	dihydrolipoamide dehydrogenase	8778521	*Arabidopsis thaliana*	53.75/6.96	56.91/6.88	5.58 ± 1.42
37	dihydrolipoamide succinyl transferase	49659786	*Cynodon dactylon*	17.96/4.91	45.05/6.41	2.34 ± 0.34
13	malic enzyme	228412	*Populus trichocarpa* × *Populus deltoides*	64.97/6.36	68.5/6.56	2.56 ± 0.20
14	malice enzyme 1	15225262	*Arabidopsis thaliana*	64.24/6.32	69.31/6.70	5.68 ± 1.41
			Isoprenoid Metabolism (9.3%)			
33	putative acetyl CoA acetyltransferase	47848479	*Oryza sativa*	41.00/6.15	41.70/6.89	2.12 ± 0.13
51	isopentenyl diphosphate isomerase 1	13603406	*Nicotiana tabacum*	33.18/5.94	28.0/5.25	3.35 ± 0.18
24	prenyltransferase domain containing protein	215694601	*Oryza sativa*	67.64/6.77	40.50/5.35	3.13 ± 0.61
15	dimethylmenaquinone methyltransferase	15237348	*Arabidopsis thaliana*	17.81/5.42	17.2/5.52	4.17 ± 0.31
			Fatty Acid Synthesis (7.0%)			
29	β-ketoacyl-ACP synthetase I	115466908	*Oryza sativa*	49.02/6.76	46.03/6.51	2.03 ± 0.22
32	β-ketoacyl-ACP synthetase I	115466908	*Oryza sativa*	49.02/6.76	46.5/6.68	3.65 ± 0.95
34	β-ketoacyl-ACP synthetase I	115466910	*Oryza sativa*	49.02/6.76	47.00/6.82	3.46 ± 0.36
			Protein Hydrolysis (7.0%)			
36	metallopeptidase	15218027	*Arabidopsis thaliana*	48.23/6.25	46.71/6.07	+
47	26S proteasome regulatory subunit rpn11	115435850	*Oryza sativa*	34.32/6.12	32.53/6.82	+
57	cysteine proteinase	18422289	*Arabidopsis thaliana*	51.17/5.86	30.52/4.98	4.27 ± 0.30
			Defense Responses (23.2%)			
17	thaumatin-like protein	17978815	*Daucus carota*	22.07/4.90	27.92/4.95	10.24 ± 1.27
43	putative thaumatin-like protein	27261063	*Oryza sativa*	25.67/4.85	27.8/5.10	2.31 ± 0.02
6	pathogenesis-related protein 4	2738609	*Dioscorea bulbifera*	16.47/5.58	12.6/5.13	4.40 ± 0.30
39	pollen allergen Bet v1	1542867	*Betula pendula*	17.45/5.81	14.6/6.30	2.42 ± 0.53
25	acidic endochitinase	115441183	*Oryza sativa*	31.47/6.30	27.11/5.48	2.56 ± 0.33
52	acidic endochitinase	115441183	*Oryza sativa*	31.47/6.30	26.8/5.98	2.03 ± 0.26
45	class III acidic chitinase	10954033	*Malus* × *domestica*	31.60/4.80	27.45/5.24	9.64 ± 1.73
55	secoisolariciresinol dehydrogenase	13752458	*Forsythia* × *intermedia*	29.24/6.16	28.6/6.08	2.14 ± 0.63
53	hypersensitive induced reaction 3	162462908	*Zea mays*	31.53/5.82	27.6/5.95	2.57 ± 0.53
23	putative adenosine kinase	41350585	*Populus alba* × *P. tremula*	24.99/6.02	39.80/5.34	4.01 ± 0.87
			Oxidative Stress (11.6%)			
26	monodehydroascorbate reductase I	51860738	*Pisum sativum*	47.32/5.79	44.2/6.45	2.26 ± 1.08
27	monodehydroascorbate reductase	4666287	*Oryza sativa*	46.63/5.53	45.87/6.45	2.95 ± 1.18
38	2-Cys peroxiredoxin	15131688	*Pisum sativum*	28.85/5.98	23.1/5.18	2.41 ± 0.15
54	cytosolic ascorbate peroxidase	14324146	*Suaeda maritime*	27.42/5.38	27.0/6.10	4.43 ± 1.00
58	glutathione peroxidase2	15225103	*Arabidopsis thaliana*	18.93/5.60	16.7/6.08	+
			Miscellaneous (16.3%)			
10	chaperonin TCP-1	15229866	*Arabidopsis thaliana*	59.74/6.03	66.02/6.85	+
16	eukayotic translation initiation factor 5A-1	15223002	*Arabidopsis thaliana*	17.35/5.41	16.7/5.62	4.12 ± 0.66
59	translationally controlled tumor protein-like protein	21595816	*Arabidopsis thaliana*	18.87/4.52	20.03/4.56	2.32 ± 0.26
46	2-isopropylmalate synthase A	7387848	*Solanum pennellii*	64.32/5.66	64.35/6.23	2.09 ± 0.27
9	RuBisCO small subunit 5	585790	*Mesembryanthemum crystallinum*	20.17/6.73	22.41/6.39	+
49	ribulose 1,5-bisphosphate carboxylase/oxygenase	20530990	*Diphyscium longifolium*	50.41/6.05	28.89/5.79	+
8	unknow protein	18400436	*Arabidopsis thaliana*	19.57/9.18	13.09/5.19	9.26 ± 1.20

[a] Relative up-accumulated fold was calculated as the ratio of spot intensities for fully ripe stage with respect to the green one. + indicates detection only in the fully ripe fruit. Values represent mean ± SE. [b] The percentage of identified proteins in each functional category.

6-phosphate isomers of α-D-glucose (*11*). Triose-phosphate isomerase (EC 5.3.1.1) catalyzes the isomerization of dihydroxyacetone phosphate and glyceraldehyde 3-phosphate (*5*, *10*). The accumulation of these four enzymes was increased during autumn olive fruit ripening (**Table 2**), in agreement with observations in ripening banana (*20*), citrus (*11*), and tomato (*5*, *10*). The results

indicate their direct or indirect responsibility, at least partly, for significant amounts of glucose and fructose during autumn olive fruit ripening.

Altogether, these glycolytic enzymes were highly accumulated, implying that the soluble sugar mainly rose from the hydrolysis of starch and sucrose into glucose and fructose within the fruit itself during autumn olive fruit ripening.

Proteins Related to Organic Acid Metabolism. Organic acids are one of the important factors influencing fruit taste (*21*). As **Table 1** shows, total organic acid content was 26.59 ± 1.63 mg/g fresh weight in the fully ripe autumn olive fruit, which was similar to that of the sweet cherry (*7*), but higher than that of tomato (*16*, *22*). Malic acid was the principal organic acid in the green autumn olive fruit, accounting for about 51% of the total acid concentration, and showed little change. Malic acid was also found to be the major organic acid (1.24 ± 0.04%) in the sweet cherry, but it accumulated during cherry ripening (*7*). Citric acid was the second most abundant organic acid, and significantly ($p < 0.01$) increased with the ripening. Lactic acid and tartaric acid were other acid components detected in autumn olive. Tartaric acid content decreased significantly ($p < 0.05$), whereas lactic acid concentration did not change significantly throughout the ripening period (**Table 1**).

In our study, four up-accumulated proteins potentially involved in malic and citric acid metabolism were identified, including dihydrolipoamide dehydrogenase 1 (spot 11), putative dihydrolipoamide succinyl-transferase (spot 37), and two malic enzymes (spots 13 and 14) (**Table 2**). Dihydrolipoamide dehydrogenase (EC 1.8.1.4) and dihydrolipoamide succinyltransferase (EC 2.3.1.61) are the subunits of 2-oxoglutarate dehydrogenase complex, which constitutes a mitochondrially localized tricarboxylic acid cycle multienzyme system responsible for the conversion of 2-ketoglutarate to succinyl-CoA and CO_2 (*11*). Malic enzyme (EC 1.1.1.40) catalyzes the oxidative decarboxylation of malic acid to pyruvate and CO_2 (*10*, *11*). As expected, the levels of malic acid were dramatically reduced in the overexpressing transgenic lines (*23*). The organic acid content of ripe fruit is determined by the net balance of acid synthesis, degradation, utilization, and compartmentalization (*21*). In the present study, the sharp accumulation of 2-oxoglutarate dehydrogenase complex and malic enzyme (**Table 2**) could be associated with dynamic balance of malic acid content and the increase of citric acid concentration during autumn olive fruit ripening.

Proteins Associated with Isoprenoid Metabolism. Special interest has been shown in autumn olive fruit due to its exceptionally high content of lycopene, a powerful antioxidant. As expected, three proteins associated with upstream isoprenoid metabolism of carotenoid biosynthesis were identified here. Acetyl-CoA C-acetyltransferase (EC 2.3.1.9) catalyzes a reversible Claisen-type condensation of two acetyl-CoA molecules to form acetoacetyl-CoA, the first step of the mevalonate pathway (*9*). Mevalonate can be converted to 3-isopentenyl diphosphate (IPP). IPP isomerase (EC 5.3.3.2) catalyzes isomerization between IPP and dimethylallyl diphosphate, both of which are essential precursors for terpenoid biosynthesis (*24*). Then prenyltransferase (EC 2.5.1.−) condenses dimethylallyl diphosphate successively with three IPP molecules to produce geranylgeranyl diphosphate (GGPP) (*25*). It has been found that the activity of IPP isomerase in *Escherichia coli* is a limiting step for carotenoid production. *E. coli* engineered with different plant, algal, or yeast IPP isomerase genes showed enhanced accumulation of carotenoids (*26*). All three genes have been identified in tomato fruit (U217603, ACS34993.1, and U75644), a main source of lycopene, but their protein expression changes during tomato fruit ripening are unknown. In this study, three isoprenoid metabolism proteins (spots 33, 51, and 24) were found to be significantly up-accumulated during fruit ripening (**Table 2**). Our previous result showed that lycopene in autumn olive fruit was highly regulated by the coordination of the expression among carotenogenic genes during fruit ripening, which were GGPP synthase, phytoene synthase, phytoene desaturase, ζ-carotene desaturase, lycopene β-cyclase, lycopene ε-cyclase, and β-carotene hydroxylase (*3*). Because GGPP is the precursor of the carotenoids, the increased accumulation of these three enzymes in isoprenoid metabolism may contribute to high lycopene content, which increased dramatically and reached 1822 μg/g dry weight and accounted for about 98% of the total carotenoids in the fully ripe fruit (*3*).

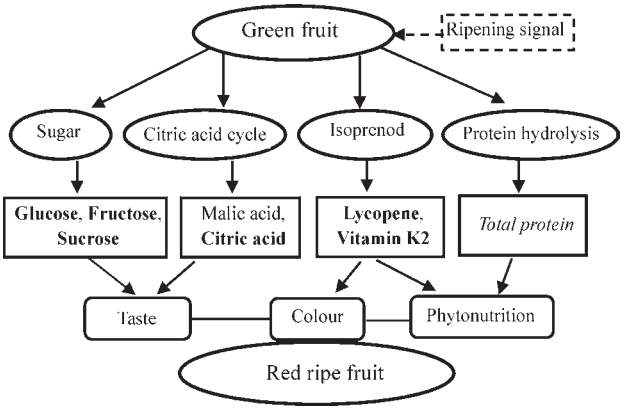

Figure 3. Simple schematic representation of induced physiological processes associated with fruit quality during autumn olive fruit ripening. Metabolites in bold font accumulated significantly during fruit ripening; those in italics decreased, and those in regular font were unchanged.

The accumulation level of demethylmenaquinone methyltransferase (spot 15) increased >4-fold during autumn olive fruit ripening (**Table 2**). This enzyme (EC 2.1.1.−) catalyzes the transfer of a methyl group to demethylmenaquinone in the final step of menaquinone (vitamin K_2) formation that has side chains composed of a variable number of unsaturated isoprenoid residues (*27*). This is the first time that the protein expression change of demethylmenaquinone methyltransferase has been observed during fruit ripening.

Lycopene is the most potent antioxidant among the carotenoids of plant sources (*28*), and vitamin K_2 is the most biologically active form of vitamin K and plays a crucial role in many bodily functions (*27*). On the other hand, lycopene is a pigment and gives autumn olive fruit its deep red color (*1*).

Other Proteins. Three protein spots (spots 29, 32, and 34) corresponding to β-ketoacyl-ACP synthetase I (EC 2.3.1.41), which is generally responsible for catalyzing a series of reactions that sequentially adds a C_2 unit derived from malonyl moiety to the growing fatty acid chain in type II fatty acid synthesis (*9*), were also found to be up-accumulated in ripening autumn olive fruit (**Table 2**). In contrast, the intensity of this protein was decreased during grape ripening (*9*).

Another three proteins characterized here were involved in protein hydrolysis (spots 36, 47, and 57). Metallopeptidase (EC 3.4.24.−) catalyzes the hydrolysis of peptide bonds by a mechanism in which water acts as a nucleophile, one or two metal ions hold the water molecule in place, and charged amino acid side chains are ligands for the metal ions (*29*). 26S proteasome is involved in the ATP-dependent degradation of ubiquitinated proteins (*29*). In this study, both metallopeptidase and 26S proteasome regulatory subunit RPN11 were first identified to respond to fruit ripening and detected only in the fully ripe

autumn olive fruit (**Table 2**), thereby being newly synthesized proteins. Cysteine or thiol proteinase (EC 3.4.22) catalyzes the hydrolysis of peptide bonds within proteins and contains a cysteine residue in the active site (http://www.yeastrc.org/pdr/). The protein was markedly up-accumulated >4-fold in autumn olive fruit by ripening (**Table 2**), whereas a smaller increase was observed in tomato fruit (*12*). The strong accumulation of three proteolytic proteins may result in reducing protein accumulation. Indeed, total protein content decreased significantly ($p < 0.05$) from 1.62 ± 0.03 mg/g at green stage to 1.27 ± 0.09 mg/g fresh weight at fully ripe stage, which was little higher than that of cherry tomato pericarp (*12*).

A simple model outlining the linking perception of a ripening signal to biochemical events such as the metabolism of sugar, organic acid, terpenoid, and protein is shown in **Figure 3**. To our knowledge, this study was the first to examine the major changes of soluble sugar and organic acid composition and protein accumulation in autumn olive fruit during ripening. Because all of the protein identifications were based on the homology with those of other plant species, determined peptide sequences may provide useful information for future gene cloning and functional studies.

ACKNOWLEDGMENT

We gratefully thank Dr. Min Wu (University of Arizona) for critical reading and grammatical correction of the manuscript.

Supporting Information Available: Table S1, spot ID, identified protein, accession number, source organism, protein score, protein score CI %, amino acid sequence coverage for the identified proteins by PMF and MS/MS, number of matched peptides by MS/MS, total ion score, parent ions, sequences of the matched peptides, and PMF and MS/MS spectra for single matched peptide; Table S2, PMF and MS/MS spectra for the spots that had more than one matched peptide. This material is available free of charge via the Internet at http://pubs.acs.org.

LITERATURE CITED

(1) Fordham, I. M.; Zimmerman, R. H.; Black, B. L.; Clevidence, B. M.; Wiley, E. R. Autumn olive: a potential alternative crop. *Acta Hortic.* **2003**, *626*, 437−439.

(2) Ahmad, S. D.; Sabir, S. M.; Zubair, M. Ecotypes diversity in autumn olive (*Elaeagnus umbellata* Thunb): a single plant with multiple micronutrient genes. *Chem. Ecol.* **2006**, *22*, 509−521.

(3) Guo, X. L.; Yang, L.; Hu, H. T.; Yang, L. Cloning and expression analysis of carotenogenic genes during ripening of autumn olive fruit (*Elaeagnus umbellata*). *J. Agric. Food Chem.* **2009**, *57*, 5334−5339.

(4) Brady, C. J. Fruit ripening. *Annu. Rev. Plant Physiol.* **1987**, *38*, 155−178.

(5) Rocco, M.; D'Ambrosio, C.; Arena, S.; Faurobert, M.; Scaloni, A.; Marra, M. Proteomic analysis of tomato fruits from two ecotypes during ripening. *Proteomics* **2006**, *6*, 3781−3791.

(6) Benard, C.; Gautier, H.; Bourgaud, F.; Grasselly, D.; Navez, B.; Caris-Veyrat, C.; Weiss, M.; Gneard, M. Effects of low nitrogen supply on tomato (*Solanum lycopersicum*) fruit yield and quality with special emphasis on sugars, acids, ascorbate, carotenoids, and phenolic compounds. *J. Agric. Food Chem.* **2009**, *57*, 4112−4123.

(7) Serrano, M.; Guillén, F.; Martínez-Romero, D.; Castillo, S.; Valero, D. Chemical constituents and antioxidant activity of sweet cherry at different ripening stages. *J. Agric. Food Chem.* **2005**, *53*, 2741−2745.

(8) Guarino, C.; Arena, S.; De Simone, L.; D'Ambrosio, C.; Santoro, S.; Rocco, M.; Scaloni, A.; Marra, M. Proteomic analysis of the major soluble components in Annurca apple flesh. *Mol. Nutr. Food Res.* **2007**, *51*, 255−262.

(9) Giribaldi, M.; Perugini, I.; Sauvage, F. X.; Schubert, A. Analysis of protein changes during grape berry ripening by 2-DE and MALDI-TOF. *Proteomics* **2007**, *7*, 3154−3170.

(10) Negri, A. S.; Prinsi, B.; Rossoni, M.; Failla, O.; Scienza, A.; Cocucci, M.; Espen, L. Proteome changes in the skin of the grape cultivar Barbera among different stages of ripening. *BMC Genomics* **2008**, *9*, 378.

(11) Katz, E.; Fon, M.; Lee, Y. J.; Phinney, B. S.; Sadka, A.; Blumwald, E. The citrus fruit proteome: insights into citrus fruit metabolism. *Planta* **2007**, *226*, 989−1005.

(12) Faurobert, M.; Mihr, C.; Bertin, N.; Pawlowski, T.; Negroni, L.; Sommerer, N.; Causse, M. Major proteome variations associated with cherry tomato pericarp development and ripening. *Plant Physiol.* **2007**, *143*, 1327−1346.

(13) Moing, A.; Renaud, C.; Gaudillère, M.; Raymond, P.; Roudeillac, P.; Denoyes-Rothan, B. Biochemical changes during fruit development of four strawberry cultivars. *J. Am. Soc. Hortic. Sci.* **2001**, *126*, 394−403.

(14) Yu, C. L.; Yan, S. P.; Wang, C. C.; Hu, H. T.; Sun, W. N.; Yan, C. Q.; Chen, J. P.; Yang, L. Pathogenesis-related proteins in somatic hybrid rice induced by bacterial blight. *Phytochemistry* **2008**, *69*, 1989−1996.

(15) Yan, J. X.; Wait, R.; Berkelman, T.; Harry, R. A.; Westbrook, J. A.; Wheeler, C. H.; Dunn, M. J. A modified silver staining protocol for visualization of proteins compatible with matrix-assisted laser desorption/ionization and electrospray ionization−mass spectrometry. *Electrophoresis* **2000**, *21*, 3666−3672.

(16) Osvald, J.; Petrovie, N.; Demsar, J. Sugar and organic acid content of tomato fruits (*Lycopersicon lycopersicum* Mill.) grown on aeroponics at different plant density. *Acta Aliment.* **2001**, *30*, 153−161.

(17) Stommel, J. R.; Abbott, J. A.; Saftner, R. A. USDA 02L1058 and 02L1059: cherry tomato breeding lines with high fruit β-carotene content. *HortScience* **2005**, *40*, 1569−1570.

(18) Famlani, F.; Walker, R. P.; Tecsi, L.; Chen, Z. H.; Proietti, P.; Leegood, R. C. An immunohistochemical study of the compartmentation of metabolism during the development of grape berries. *J. Exp. Bot.* **2000**, *51*, 675−683.

(19) Yu, X.; Wang, X.; Zhang, W.; Qian, T.; Tang, G.; Guo, Y.; Zheng, C. Antisense suppression of an acid invertase gene (*MAII*) in muskmelon alters plant growth and fruit development. *J. Exp. Bot.* **2008**, *59*, 2969−2977.

(20) Junior, A. V.; do Nascimento, J. R. O.; Lajolo, F. M. Molecular cloning and characterization of an α-amylase occuring in the pulp of ripening bananas and its expression in *Pichia pastoris*. *J. Agric. Food Chem.* **2006**, *54*, 8222−8228.

(21) Chen, F. X.; Liu, X. H.; Chen, L. S. Developmental changes in pulp organic acid concentration and activities of acid-metabolising enzymes during the fruit development of two loquat (*Eriobotrya japonica* Lindl.) cultivars differing in fruit acidity. *Food Chem.* **2009**, *114*, 657−664.

(22) Carli, P.; Arima, S.; Fogliano, V.; Tardella, L.; Frusciante, L.; Ercolano, M. R. Use of network analysis to capture key traits affecting tomato organoleptic quality. *J. Exp. Bot.* **2009**, *60*, 3379−3386.

(23) Fahnenstich, H.; Saigo, M.; Niessen, M.; Zanor, M. I.; Andreo, C. S.; Fernie, A. R.; Drincovich, M. F.; Flugge, U. I.; Maurino, V. G. Alteration of organic acid metabolism in *Arabidopsis* overexpressing the maize C4 NADP-malic enzyme causes accelerated senescence during extended darkness. *Plant Physiol.* **2007**, *145*, 640−652.

(24) Okada, K.; Kasahara, H.; Yamaguchi, S.; Kawaide, H.; Kamiya, Y.; Nojiri, H.; Yamane, H. Genetic evidence for the role of isopentenyl diphosphate isomerases in the mevalonate pathway and plant development in *Arabidopsis*. *Plant Cell Physiol.* **2008**, *49*, 604−616.

(25) Séguin, A.; Gershenzon, J. A bifunctional geranyl and geranylgeranyl diphosphate synthase is involved in terpene oleoresin formation in Norway spruce (*Picea abies*). *Plant Physiol.* **2010**, *152*, 639−655.

(26) Sun, Z.; Cunningham, F. X.; Gantt, E. Differential expression of two isopentenyl pyrophosphate isomerases and enhanced carotenoid

accumulation in a unicellular chlorophyte. *Proc. Natl. Acad. Sci. U.S.A.* **1998**, *95*, 11482−11488.
(27) Widhalm, J. R.; van Oostende, C.; Furt, F.; Basset, G. J. C. A dedicated thioesterase of the Hotdog-fold family is required for the biosynthesis of the naphthoquinone ring of vitamin K1. *Proc. Natl. Acad. Sci. U.S.A.* **2009**, *106*, 5599−5603.
(28) Agarwal, S.; Rao, A. V. Tomato lycopene and its role in human health and chronic diseases. *Can. Med. Assoc. J.* **2000**, *163*, 739−744.
(29) Beers, E. P.; Woffenden, B. J.; Zhao, C. Plant proteolytic enzymes: possible roles during programmed cell death. *Plant Mol. Biol.* **2000**, *44*, 399−415.

Received for review June 22, 2010. Revised manuscript received December 5, 2010. Accepted December 7, 2010. This research was funded by National Natural Science Foundation of China (31071775), the Science and Technology Department of Zhejiang Province (2008C24006), and the Zhejiang Normal University Innovative Research Team Program China.